Electronic Supplementary Material (ESI) for Energy & Environmental Science.
This journal is © The Royal Society of Chemistry 2023

Efficiency limits and design principles for multi-junction coloured photovoltaics

Supplementary Information

Phoebe M. Pearce [a], Janne Halme [b], Jessica Yajie Jiang [a], and Nicholas J. Ekins-Daukes [a]

1. Perceived colour calculations

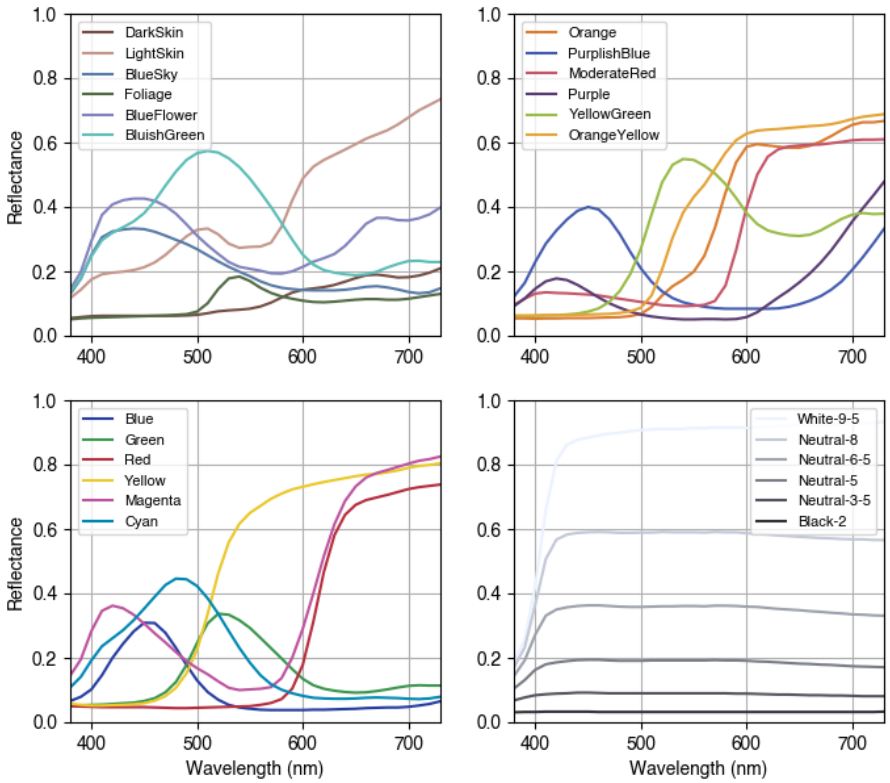

Figure S1. Reflectance spectra for the ColorChecker colours, averaged from 30 measurements of real charts. Data from [1]. The grouping of the colours in different plots has no significance and is done for clarity.

The target *(X, Y, Z)* coordinates for the optimization are calculated using the reflectance spectra in Figure S1 and assuming an object with this reflectance is illuminated with an AM1.5G spectrum (Figure S2). For visual representation, these colours are converted to sRGB coordinates using the D65 illuminant. This choice of target *(X, Y, Z)* coordinates differs from Halme & Mäkinen [2] who used the "BabelColor Avg." *xyY* coordinates for CIE D50 illuminant (average of 20 charts) from [3] as the target colour coordinates for the colour optimization. [2] also used the CIE D65 illuminant to transfer to sRGB coordinates for visual representation, and the AM1.5G spectrum for the solar cell efficiency calculations. Here, using the reflectance data from [1], we performed all colourimetric and photovoltaic calculations self-consistently with the AM1.5G spectrum. If using the same target coordinates as [2], the same results are obtained, as shown in Figure S6.

[a] School of Photovoltaic and Renewable Engineering, University of New South Wales, Sydney, New South Wales 2052, Australia

[b] Department of Applied Physics, Aalto University School of Science, P.O. Box 15100, 00076 Aalto, Finland.

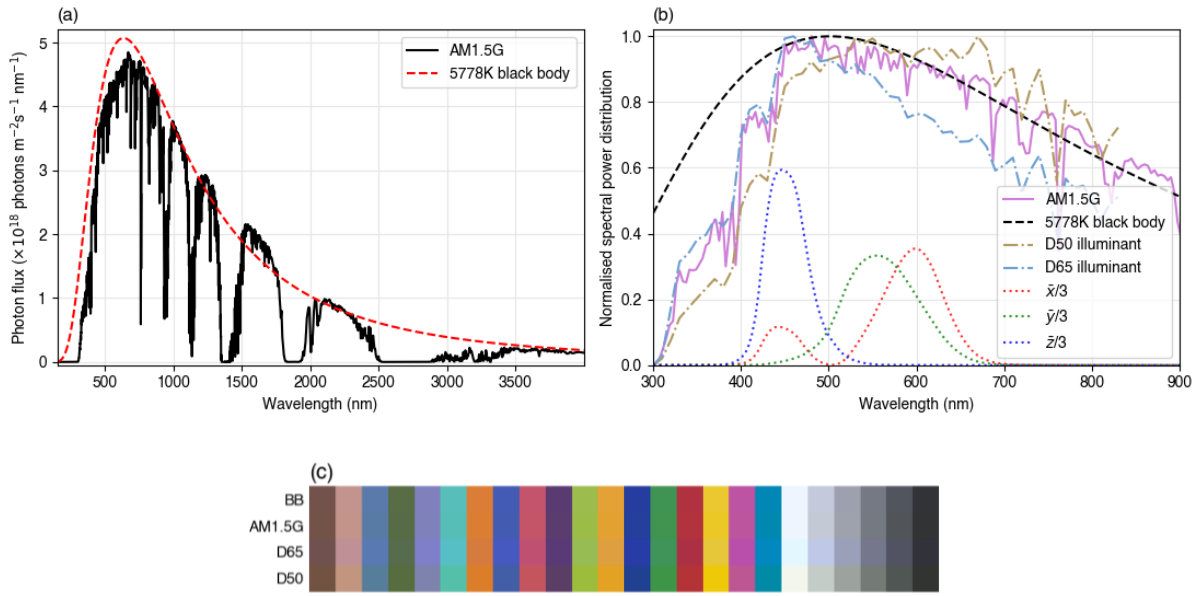

Figure S2. (a) Photon flux as a function of wavelength in the AM1.5G [4] spectrum and a black body at 5778K occupying a solid angle of 6.8×10^{-5} (the average solid angle of the Sun as viewed from Earth). (b) Different "white light" illuminants: AM1.5G, a Sun-like black body, and the CIE standard illuminants [5] D50 and D65. D65 is intended to represent average daylight with a colour temperature of 6500K, and is thus slightly 'bluer' than AM1.5G/a 5778K black body spectrum, while D50 has a colour temperature of 5000K and thus appears more red. (c) sRGB calculated colours when optimized reflectance spectra (targeting the ColorChecker colours) are illuminated with the listed illuminant. The reflectance spectrum is the same for each colour across illuminants. The target illuminant (i.e. for viewing the sRGB colours) was assumed to be D65 in each case.

2. Differential evolution

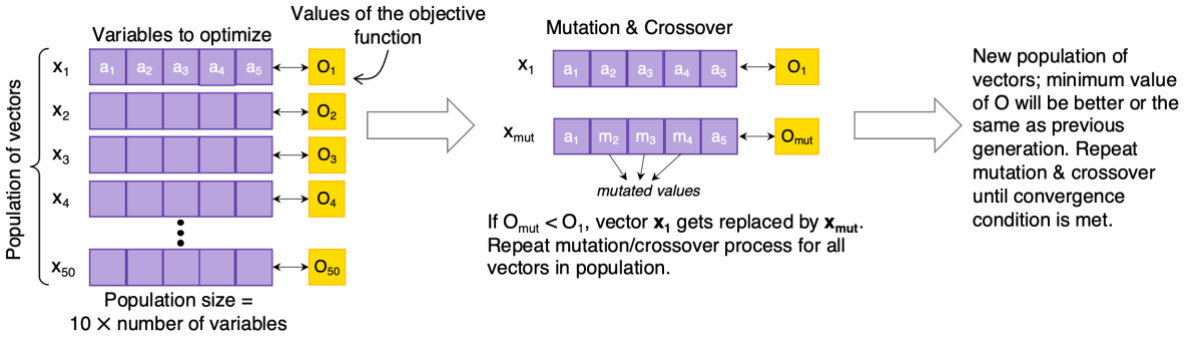

Figure S3. Basic operation of a differential evolution optimization algorithm.

A. Details of multi-objective differential evolution procedure

Variable bounds

- *Centre of reflectance peaks*: 380-730 nm (visible wavelength range)
- *Width of reflectance peaks*: The lower limit is 0 nm (i.e. no peak). The upper limit is the maximum of the values:

$$w_{upper} = \max\left(\left\{\frac{160}{n_{peaks}}, \frac{350}{n_{peaks}}Y\right\}\right)$$

  where n_{peaks} is the number of rectangular reflectance peaks with 100% reflectance and Y is the relative luminance of the target colour. The rationale for these limits is that the widest reflectance band, which covers the whole visible spectrum and produces a colour with $Y = 1$ (i.e. the reference white value), would have a width of 350 nm; we divide by the number of peaks since the peaks can be placed anywhere in the visible range, and thus the maximum total width we would want is 350 nm for $Y = 1$. Darker colours (lower Y) will require narrower bands. To avoid making the upper limit too low for colours with relatively low Y but which require more photons near the peak of one of the colour matching functions to produce the desired hue, the maximum total width of the reflectance bands is always at least 160 nm.
- *Bandgaps*: Optimization of coloured cells with N junctions is preceded by optimization of a cell with 0% reflectance (i.e. a black cell) with N junctions. The bandgap of each junction in the optimization of the coloured cell is bounded between $0.6E_{g,\,black}$ and $1.2E_{g,\,black}$. Note that the lower limit is further from the black cell value because any introduction of colour is expected to reduce the optimal bandgaps [2].

Differential evolution settings

The standard settings for the multi-objective differential evolution solver in pygmo [6] (referred to internally as `moead`: Multi-Objective Evolutionary Algorithm based on Decomposition) were used:

- `CR = 1`
- `F = 1`
- `eta_m = 20`
- `weight_generation = “grid”`
- `decomposition = “tchebycheff”`

- `diversity_preservation = True`

A basic schematic outline of how the differential evolution proceeds is shown in Figure S3. Further details of the mutation and crossover method used can be found in [7], which also describes how the parameters `CR`, `F` and `eta_m` (η) are used. Qualitatively, `CR` controls the probability for each vector element to be replaced by its mutated version, while `F` controls the 'strength' of the mutation. The decomposition and weight generation settings control how the multi-objective problem is decomposed into single-objective sub-problems. Note that apart from setting `F` = 1 (default `F` = 0.5), pygmo's default settings were used since they give good results in terms of convergence and speed of the optimization; further experimentation with these parameters could likely improve these further.

With reference to Figure 3 in the main text, the parameters used for our specific implementation of the multi-objective DE method are:

- Population size on each island is 10 times the number of variables to optimize, n_{vars} (reflectance peak locations and widths, and bandgaps. For example, a two-junction cell with two rectangular reflectance peaks has 6 variables: 2 peak locations, 2 peak widths, and 2 bandgaps).
- $n_{iter} = 50n_{vars}$ (number of iterations/generations which are run separately on each island in each batch)
- $I = 10$ (the number of islands, i.e. parallel processes running separate optimizations)
- $\Delta XYZ_{max} = 0.004$ (the maximum allowed colour deviation, defined by equation 2 in the main text)
- $\Delta\eta_{threshold} = 1 \times 10^{-5}$ percentage points (optimization will end if the change in best efficiency between batches of n_{iter} generations is less than this)
- $N_{reset} = 2$ (at the end of each batch, all islands are sorted by highest efficiency within ΔXYZ_{max}, and the populations of the N_{reset} worst-performing islands are reset the same way as the start of the optimization process).

If the colour threshold is not met by any population members at the end of n_{iter}, the algorithm will automatically continue. If after 3 batches of iterations (300 total iterations with the settings used), it is assumed the colour cannot be produced by reflecting the illuminant and the optimization is halted. Since the optimization proceeds in batches of iterations, comparing the best efficiency at the end of the batch to see if it has improved, there will always be a minimum of $2 \times 50 \times n_{vars}$ total iterations (two batches of $50 \times n_{vars}$ iterations). The number of iterations per batch can also be reduced to speed up the optimization for less strict convergence conditions.

To more efficiently use the vector population to search for acceptable solutions, the multi-objective problem was constrained to only search with $\Delta XYZ \leq 0.05$ (compared to $\Delta XYZ_{max} = 0.004$, at which the colour is deemed to be the same as the target colour). This is done inside the objective function by setting the cell efficiency η to 0 manually if the value of ΔXYZ exceeds 0.05; if the problem is not constrained in this way, the multi-objective optimization will generate solutions across the full range $\Delta XYZ \cong 0$ to $\Delta XYZ \cong 1$, as shown in the next sub-section. It was found that constraining the front to colours which are relatively close to the target colour gave improved convergence, especially for high numbers of junctions; however, constraining the

front too much (for example, so that all the vectors stay within $\Delta XYZ \leq 0.004$) appears to a lead to a quick loss of diversity within the population and worse convergence.

B. Examples of initial populations and non-dominated fronts

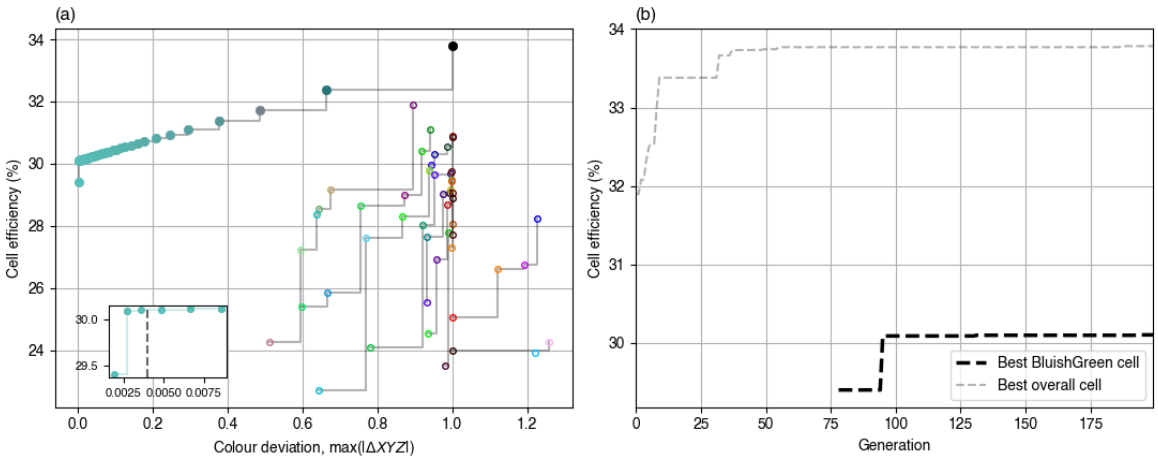

Figure S4. (a) Initial population of vectors (open circles) and final population after 200 iterations (filled circles) in a differential evolution optimization targeting a single-junction Bluish Green solar cell, represented by the value each vector gives for both objective functions (colour deviation and cell efficiency). The colour of the symbols shows the calculated perceived colour resulting from the reflectance spectrum corresponding to each vector. The inset shows the region of low colour deviation; the dashed line indicates the cut-off used in calculating the results presented in the paper (0.004). (b) The overall highest efficiency in the vector population (grey line), and the population of the most efficient cell below the cut-off colour deviation, i.e. the most efficient cell which meets the target colour (black line). The overall highest efficiency approaches the limiting efficiency of a black cell under AM1.5G. Note that there are no values for the best Bluish Green cell efficiency initially, because no population members meet the colour target.

Figure S4 shows an example of how the population of vectors in the multi-objective (cell colour and efficiency) differential evolution problem evolves from the initial population, which is randomly generated within the variable bounds. The evolution can be viewed in full in the supplementary video files.

We see that while the initial population has a wide range of efficiencies and colour deviations, the final population lies along a single line connecting a point of low efficiency and high colour accuracy (in this case, a Bluish Green solar cell) with a point of high efficiency and low colour accuracy (i.e. a black cell). Connecting these two extremes are other vectors (candidate solutions) in the final population which trade off one of the objectives against the other; as we move along the front, we can improve on one objective, but not the other. If the optimization has converged, this set of solutions represents a Pareto front; this is a set of solutions where at any point on the front, one of the objectives can only be improved by reducing performance against the other objective.

Notably, the colours along the Pareto front are all a similar hue, getting darker as the efficiency increases. The colour distance metric used during the optimization (eq. 2 in the main text) is the maximum of the fractional differences of the *(X, Y, Z)* colour coordinates from their target coordinates. This has the result that along the *x*-axis of Figure S4, the fractional differences in *X*, *Y* and *Z* tend to be approximately the same. If the three coordinates increase at the same rate along the front, this has the effect of keeping the *x* and *y* coordinates (eq. 3 in the main text) approximately constant (until the value of *Y* reaches 0, i.e. a black cell), resulting in colours of the same hue but varying luminance. To illustrate the meaning of the Pareto front, the results in Figure S4 are not restricted to only small values of ΔXYZ; as discussed above, for the results presented in the main text, the front was restricted to values of ΔXYZ less than 0.05, to more

efficiently use the populations to explore suitable solutions, rather than those very far from the target colour.

While we used strict stopping criteria and low colour deviation cut-off (see ESI Section 4A) to calculate limiting efficiencies, this may not be feasible or necessary when using more realistic optical and cell models. Figure S4 shows that once a population with acceptable colour is found, the DE method rapidly approaches the maximum efficiency, so that even a relatively small number of iterations can be used to explore a large parameter space.

C. Uncertainty estimates

Table S1. Standard deviation of the optimized efficiency across 20 runs of the optimization algorithm for a cell with *N* junctions, and two allowed reflectance peaks. The colours considered are Blue, Red, Green, Orange Yellow and Neutral 8 from the ColorChecker chart; the standard deviation given here is the highest value seen across all the colours for a given number of junctions.

N	Highest standard deviation in optimized efficiency (percentage points)
1	0.0013
2	0.0007
3	0.0009
4	0.0009
5	0.0014
6	0.0036

While evolutionary algorithms such as DE allow us to search a large parameter space and can optimize functions which are discontinuous and/or non-differentiable, they are not guaranteed to reach the absolute minimum of a function. To test the robustness of the optimization, we took a sub-set of colours with varying luminance *Y* and hue (Blue, Red, Green, Orange Yellow and Neutral 8) from the ColorChecker chart and repeated the full optimization process 20 times, for 1-6 junctions (with 2 reflectance peaks). Figure S5 and Table S1 shows the results of the 20 separate optimization runs. As the number of variables to optimize increases (more junctions or more reflectance bands), the deviation of the maximum efficiency between runs generally increases, as it becomes harder to find the optimal solution; however, even with the maximum deviation observed for six junctions (10 variables to optimize) was an absolute efficiency difference of 0.02% between the best and worst runs, for a Green cell with 6 junctions.

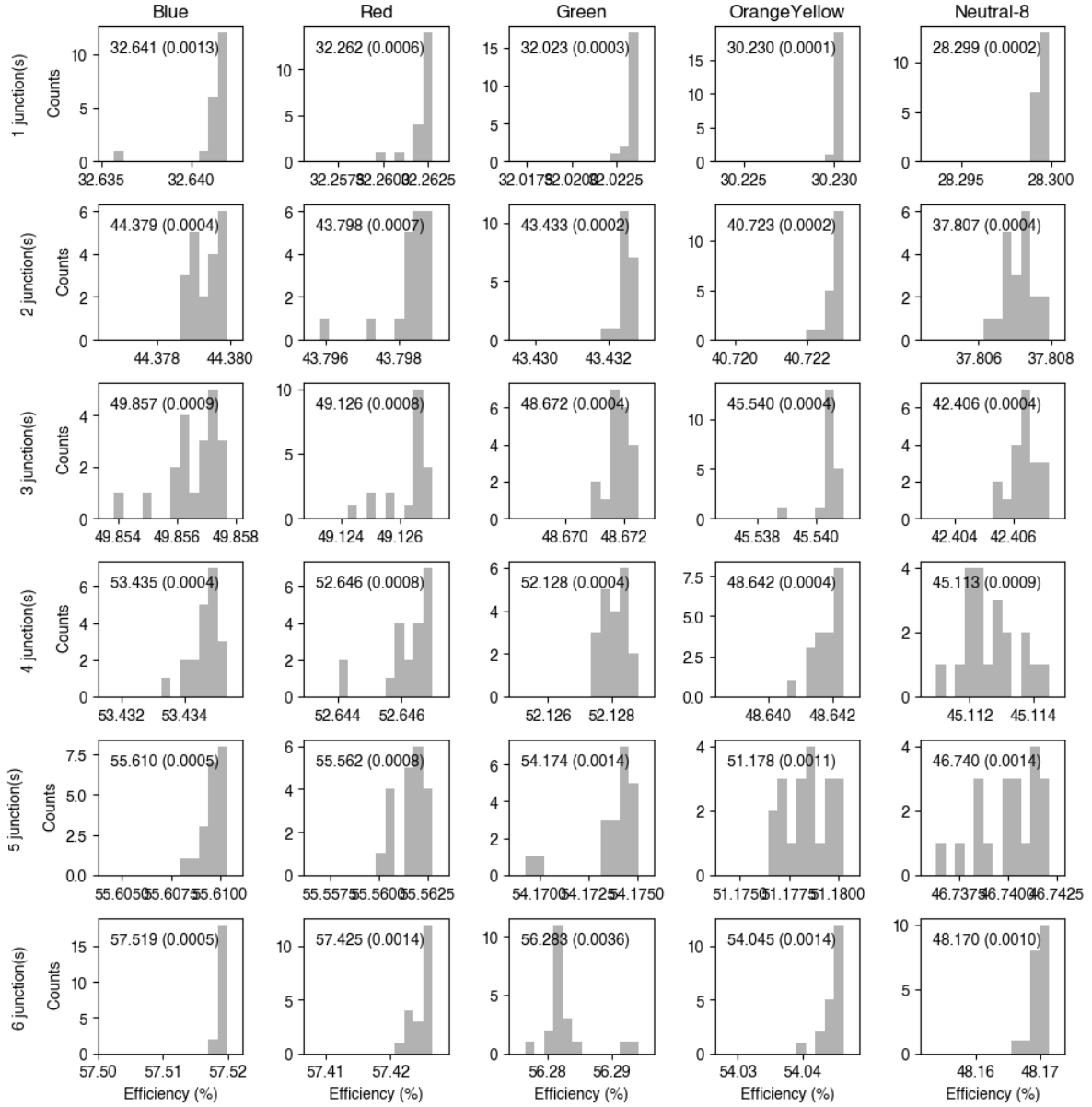

Figure S5. Distribution of the maximum efficiency obtained for five different colours, 1-6 junctions, and 2 reflectance peaks, for 20 runs of the optimization algorithm. Note that the range of the *x*-axes is fixed across colours for each junction, but the range changes with the number of junctions. The mean and standard deviation across the 20 runs are printed in each sub-plot. The highest standard deviation observed for *N* junctions is summarized in Table S1.

D. Benchmarking against single-junction results

As discussed in ESI Section 1, slightly different target colour coordinates were used here as compared to Halme & Mäkinen [2], giving slightly different optimal efficiency and bandgap results for the limiting efficiency and optimal bandgap of single-junction coloured solar cells. However, as shown in Figure S6, if the same target colour coordinates are used with the differential evolution optimization method, the same results are obtained, despite using a different optimization method.

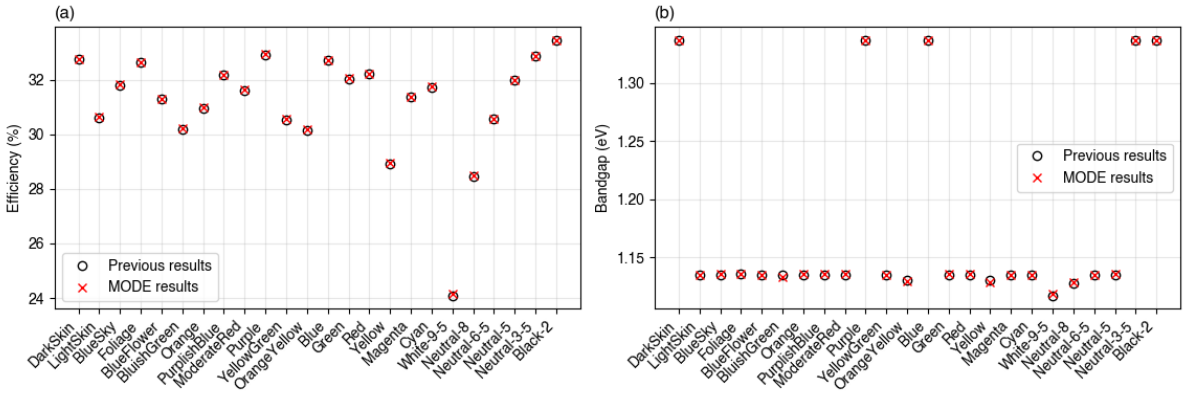

Figure S6. (a) Optimized efficiency and (b) optimized bandgap as given in [2] (black circles) and calculated using the multi-objective differential evolution (MODE) algorithm described in this paper (red crosses), when using the same target *(X, Y, Z)* used in [2].

E. Computation time

Figure S7 shows the time taken and final efficiency for optimization of cells with a range of colours for 1-3 junctions, with different value of $\Delta\eta_{threshold}$ (the acceptable change in efficiency between batches of iterations, see ESI Section 2A). The $\Delta\eta_{threshold}$ used for results presented in the main text is extremely strict (1×10^{-5} percentage points), but we see excellent convergence even with less strict conditions. All optimizations were performed on a MacBook Pro with Apple M1 Max chip, 32GB of RAM, and 10 CPU cores. As described in ESI Section A2, since the optimization proceeds in batches of iterations, comparing the best efficiency at the end of the batch to see if it has improved, there will be a minimum of $2 \times 50 \times n_{vars}$ total iterations (two batches of $50 \times n_{vars}$ iterations), and thus the total computation time will not drop below the time taken to run this many iterations, even at high values of of $\Delta\eta_{threshold}$ (non-strict convergence conditions). The time taken to execute a single cell calculation for 1-6 junctions is given in Table S2.

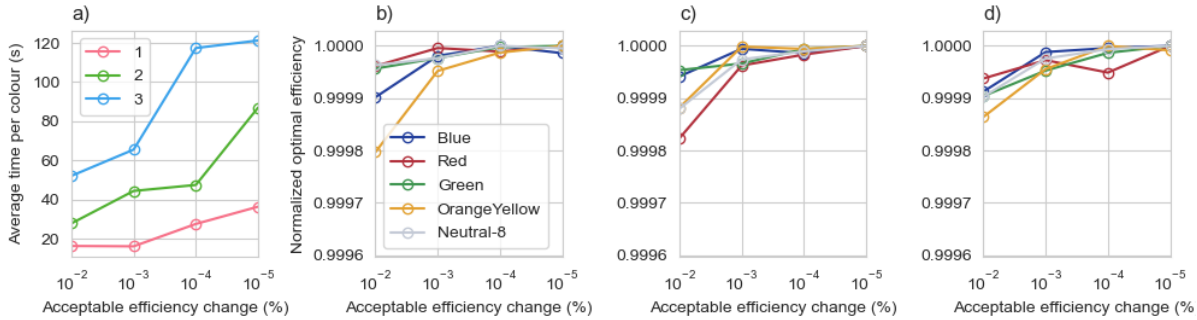

Figure S7. a) Time to reach convergence (average for five colours) with one, two or three sub-cells and different values of $\Delta\eta_{threshold}$.. b) – d) show the convergence of the maximum efficiency, normalised to the maximum efficiency seen across values of $\Delta\eta_{threshold}$ for two, three and four junctions, respectively.

Table S2. Time to execute one cell calculation for N number of junctions, assuming two rectangular reflectance peaks, using the analytical expressions for the maximum power point voltage and current.

N	Time for one calculation (s)
1	0.02
2	0.03
3	0.04
4	0.05
5	0.07
6	0.08

3. Benchmarking detailed-balance calculations

Table S3 shows a comparison of the maximum power point voltage, current density, and efficiency calculated for current-matched *N*-junction cells using the analytical model presented in the paper (An), based on [8], and by scanning through voltages (step size 0.0005 V) and finding the maximum power point numerically (Num) [9]. The cells and ambient are assumed to be at a temperature of 298 K. Note that the calculations assume a perfect reflector behind the cells; otherwise J_{01} increases by a factor of 2. We also see good agreement between our results (efficiencies and bandgaps) and those previously reported for series-connected cells under the AM1.5G spectrum in [10].

Table S3. Current density and voltage at the maximum power point, and corresponding efficiency, calculated using the analytical method (A) and by scanning through voltages (N).

N	**Bandgaps** (eV)	V_{MPP} (V)		J_{MPP} (mA/cm^2)		η (%)		$\Delta\eta$ (%)
		An	**Num**	**An**	**Num**	**An**	**Num**	
1	1.34	0.99	0.99	34.2	34.3	33.8	33.8	-0.06
2	0.96 / 1.63	1.90	1.90	24.2	24.2	45.8	45.8	-0.02
3	0.93 / 1.37 / 1.90	3.11	3.11	16.6	16.6	51.7	51.6	0.02
4	0.72 / 1.11 / 1.49 / 2.00	3.88	3.87	14.3	14.3	55.4	55.4	0.03
5	0.70 / 1.01 / 1.33 / 1.67 / 2.14	5.04	5.02	11.4	11.5	57.7	57.7	-0.02
6	0.69 / 0.96 / 1.20 / 1.47 / 1.79 / 2.24	6.17	6.10	9.62	9.75	59.3	59.5	-0.35

N = number of junctions.
η = cell efficiency
$\Delta\eta$ = relative difference between cell efficiencies calculated using analytical and numerical methods
An = analytical calculation
Num = numerical calculation

4. Supplementary results

A. Colour deviation

Colour deviation targets were quantified in the optimization using fractional deviation from the (*X, Y, Z)* coordinates, since these can be calculated very simply. However, equal differences in these coordinates do not correspond to an equal amount of colour difference as perceived by the human eye. The CIE standard uses a colour distance metric called ΔE^* [11], with a ΔE^* value of 1 generally agreed to correspond to a just-noticeable difference. For the final optimized coloured cell results with 1-6 junctions and 2 or 3 reflectance bands presented in the main text, the maximum ΔE^* calculated is 0.6. Thus, all optimized reflectance spectra should result in colours indistinguishable from the target colours.

B. Additional reflectance bands

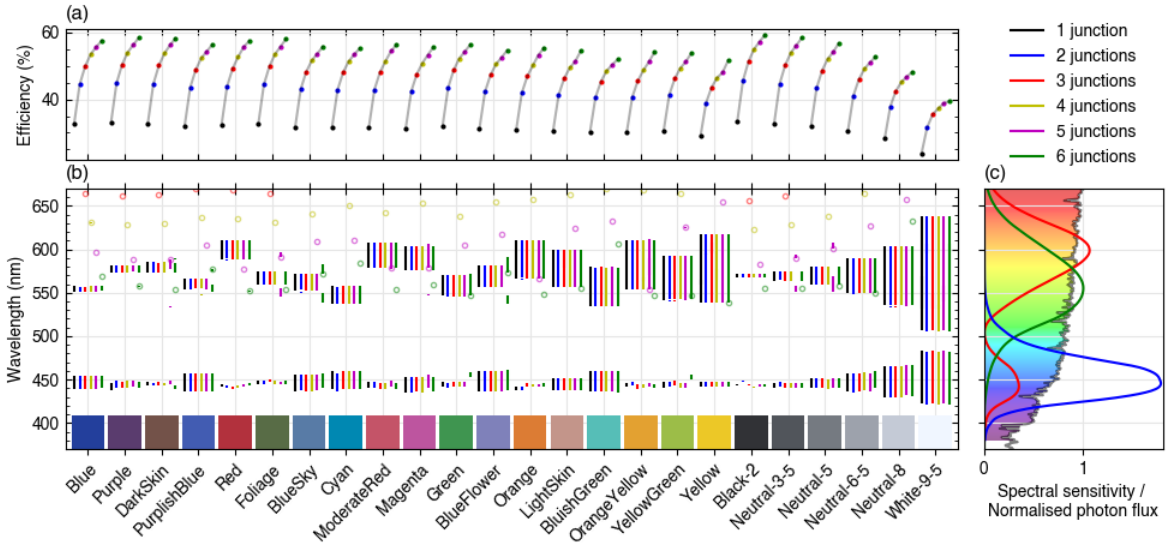

Figure S8. (a) Efficiency and (b) reflectance band placement (vertical lines) and highest bandgap (open circles) for optimized cells with 1-6 junctions for all the ColorChecker shades, allowing three peaks in the reflectance spectrum. The $\bar{x}$, $\bar{y}$ and $\bar{z}$, colour-matching functions and visible part of the AM1.5G spectrum, with indicative colours for each wavelength, are shown on the right.

As shown in Figure 5(b) of the main text, there are a small number of cases where the maximum possible efficiency of a cell with a given colour can be increased by allowing an additional third peak in the reflectance spectrum. Figure S8 shows the optimized efficiencies and reflectance spectra for 1-6 junctions when a maximum of three reflectance peaks may be used. Most of the results show two reflectance peaks, but in some cases for five or six junction cells, as the top cell bandgap moves into the visible wavelength range, maximum efficiency can be improved (by a very small amount, < 0.5% relative change) by splitting the longer-wavelength reflectance peak and placing the bandgap in between the two new peaks.

Figure S9 shows two specific examples of the optimized reflectance spectra with two vs. three allowed peaks for a cell with the colour Neutral 3-5 and five junctions, and a cell with the colour Blue Flower and six junctions. For the five-junction Neutral 3-5 case, the optimized efficiency with three allowed reflectance peaks is 56.11%, compared to 56.06% for two reflectance peaks. While the shorter-wavelength reflectance peak stays stable, the longer-wavelength peaks split into two separate peak when allowed to, with the highest sub-cell bandgap placed in between these two new peaks. This gives a slightly increased top-cell voltage at the maximum power point (1.687 V for 3 reflectance peaks vs. 1.675 V for 2 reflectance peaks, a 0.7% increase). At the same time, the top cell maximum power point current, which is the limiting current in both cases, is very slightly reduced with 3 reflectance peaks, by 0.2%, since the reflectance spectrum with 3 peaks uses slightly more photons to produce the same

colour. This same pattern also occurs in the six-junction Blue Flower cell in Figure S9(b). Since the increase in voltage is higher than the reduction in current, the overall efficiency with 3 reflectance peaks is slightly higher. However, as discussed in the main text, due to the extremely narrow and carefully-placed reflectance bands required, this effect will likely be insignificant for real devices.

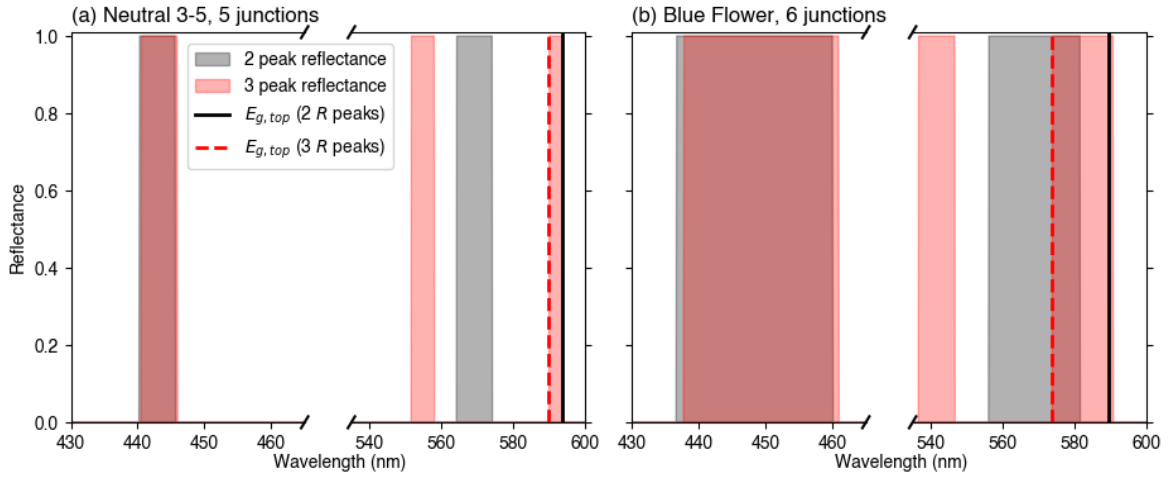

Figure S9. Optimized reflectance spectra (shaded area) and highest bandgap (vertical lines) for a (a) a five-junction cell with colour Neutral 3-5 and (b) a six-junction cell with colour Blue Flower, for two allowed reflectance peaks (grey/black) and three allowed reflectance peaks (red).

C. Optimal cell bandgaps for black body illuminant

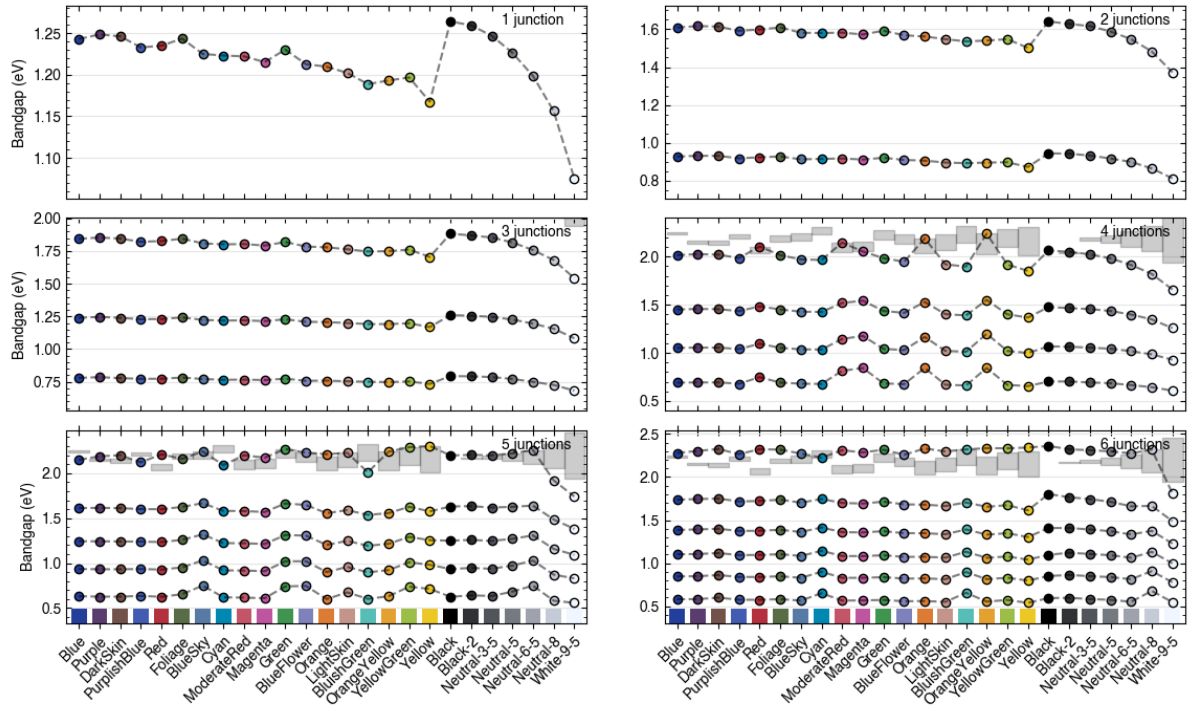

Figure S10. Optimized bandgap placement for all sub-cells for MJSCs with 1-6 junctions under a 5778K black body spectrum. The reflectance bands required to produce each colour are shown as grey-shaded areas where they fall within the same energy ranges as the bandgaps (the higher-energy reflectance peak, around 450 nm (2.76 eV) is not shown in any of the plots).

Figure S10 shows the optimal bandgap placement for cells with 1-6 junctions for the 24 ColorChecker colours and an ideal black cell, when illuminated with a Sun-like 5778K black body spectrum. Note that if an optimal bandgap falls inside a reflectance band, it is plotted at the high-energy edge of the band, as discussed in the next sub-section.

D. Bandgaps inside reflectance bands

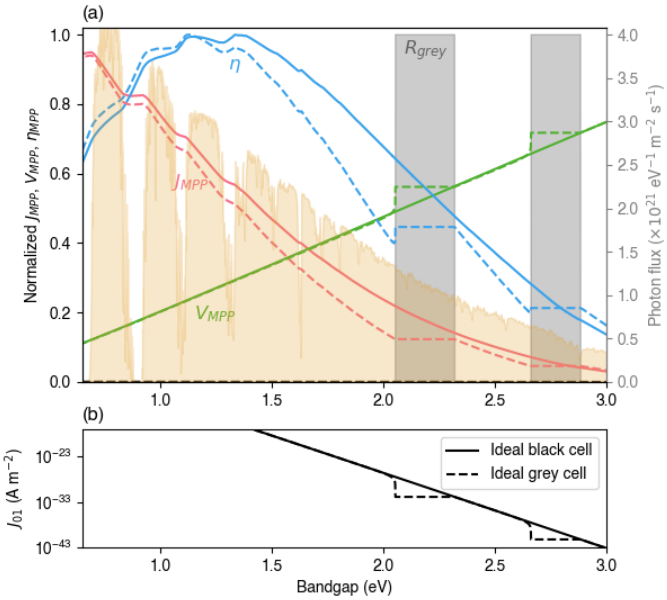

Figure S11. (a) Normalized J_{MPP}, V_{MPP} and cell efficiency η with varying bandgap for a single-junction cell for an ideal black cell (solid lines) and a grey cell with ColorChecker shade Neutral-8 (dashed lines). The photon flux in the AM1.5G spectrum (yellow shaded area) and reflectance to obtain the grey colour are also shown (grey shaded area). (b) Dark current J_{01} with bandgap for both cells.

From the definitions of the dark current and illumination current in eqs. (4) and (5) of the main text, we can see that if a bandgap is placed inside a rectangular reflectance band with height 1, there will be no effect from moving the bandgap *within* a reflectance band on either quantity. From eqn (9) of the main text, this means that V_{MPP} and I_{MPP} are also unaffected. Figure S11(a) illustrates this point, showing the current, voltage, and efficiency of the cell at the MPP as a function of bandgap for an ideal black cell with no reflectance and for a grey cell (Neutral-8). We clearly see the increase in efficiency at the edge of the reflectance bands, caused by a sudden decrease in the dark current, while J_{sc} is unchanged across the reflectance band. This effect can be explained by considering what happens when we move the bandgap from the high-energy to the low-energy edge of the reflectance band. In the detailed-balance limit, placing a sub-cell bandgap anywhere within a reflectance band is equivalent to placing it at the higher-energy edge in terms of the calculated current-voltage behaviour; since there is no absorption of photons at these bandgaps, the cell will not be emissive either, and thus it is as if the bandgap is artificially restricted to the higher-energy edge of the reflectance band. Lower-energy photons contribute exponentially more to the dark current, as shown Figure S11(b), and thus as soon as the bandgap goes below the low-energy edge of the reflectance band, the comparatively low-energy photons which will now be emitted through radiative recombination lead to a large jump (several orders of magnitude) in the dark current, leading to a rapid reduction in the voltage and thus the efficiency. Of course, if the reflectance is not 100%, as will be the case in any real cell, the magnitude of this effect is significantly reduced since there will be no single abrupt wavelength at which lower-energy photons can be emitted again, and thus this effect is unlikely to be important for real devices.

E. Effect of limiting external radiative efficiency

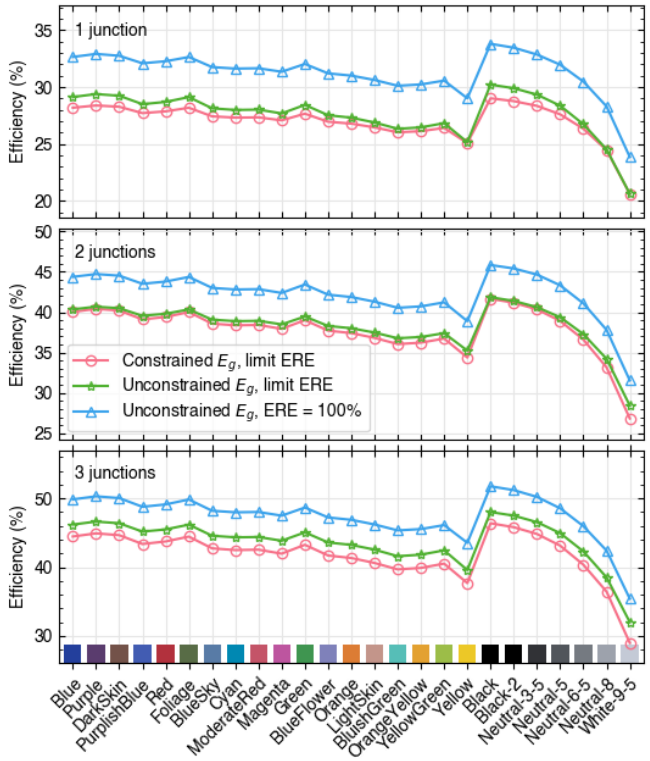

Figure S12. Limiting efficiency of cells with one to three junctions in three situations: (a) unconstrained optimization of the bandgaps, assuming 100% ERE in all junctions; (b) unconstrained optimization of the bandgaps, but setting the ERE of the bottom junction to 1.6%, and that of the additional junctions to 10%; and (c) the bottom bandgap is fixed at E_g = 1.12 eV, and the ERE values are set as in (2).

References

[1] The BabelColor Company, "ColorChecker data," BabelColor. Accessed: May 16, 2023. [Online]. Available: https://babelcolor.com/colorchecker-2.htm

[2] J. Halme and P. Mäkinen, "Theoretical efficiency limits of ideal coloured opaque photovoltaics," *Energy Environ. Sci.*, vol. 12, no. 4, pp. 1274–1285, Apr. 2019, doi: 10.1039/c8ee03161d.

[3] The BabelColor Company, "RGB coordinates of the Macbeth ColorChecker," BabelColor. Accessed: May 16, 2023. [Online]. Available: https://babelcolor.com/colorchecker-2.htm

[4] NREL, "Reference Solar Spectral Irradiance: Air Mass 1.5." Accessed: Aug. 04, 2017. [Online]. Available: http://rredc.nrel.gov/solar/spectra/am1.5/

[5] CIE, "Colorimetry - Part 2: CIE Standard Illuminants (ISO/CIE 11664-2:2022(E))." Accessed: Aug. 23, 2023. [Online]. Available: https://cie.co.at/publications/colorimetry-part-2-cie-standard-illuminants-0

[6] F. Biscani and D. Izzo, "A parallel global multiobjective framework for optimization: pagmo," *J. Open Source Softw.*, vol. 5, no. 53, p. 2338, Sep. 2020, doi: 10.21105/joss.02338.

[7] H. Li and Q. Zhang, "Multiobjective Optimization Problems With Complicated Pareto Sets, MOEA/D and NSGA-II," *IEEE Trans. Evol. Comput.*, vol. 13, no. 2, pp. 284–302, Apr. 2009, doi: 10.1109/TEVC.2008.925798.

[8] A. Pusch, P. Pearce, and N. J. Ekins-Daukes, "Analytical Expressions for the Efficiency Limits of Radiatively Coupled Tandem Solar Cells," *IEEE J. Photovolt.*, vol. 9, no. 3, pp. 679–687, May 2019, doi: 10.1109/JPHOTOV.2019.2903180.

[9] D. Alonso-Álvarez, T. Wilson, P. Pearce, M. Führer, D. Farrell, and N. Ekins-Daukes, "Solcore: a multi-scale, Python-based library for modelling solar cells and semiconductor materials," *J. Comput. Electron.*, vol. 17, no. 3, pp. 1099–1123, Sep. 2018, doi: 10.1007/s10825-018-1171-3.

[10] A. S. Brown and M. A. Green, "Detailed balance limit for the series constrained two terminal tandem solar cell," *Phys. E Low-Dimens. Syst. Nanostructures*, vol. 14, no. 1, pp. 96–100, Apr. 2002, doi: 10.1016/S1386-9477(02)00364-8.

[11] Lindbloom, "Delta E (CIE 2000)." Accessed: Aug. 23, 2023. [Online]. Available: http://www.brucelindbloom.com/index.html?Eqn_DeltaE_CIE2000.html